Low-field electron mobility in wurtzite InN

V. M. Polyakov and F. Schwierz

Articles you may be interested in

An enhancement in the low-field electron mobility associated with a ZnMgO/ZnO heterostructure: The role of a two-dimensional electron gas
J. Appl. Phys. **114**, 023703 (2013); 10.1063/1.4812492

Hole mobility in wurtzite InN
Appl. Phys. Lett. **98**, 192114 (2011); 10.1063/1.3592257

Low-field and high-field electron transport in zinc blende InN
Appl. Phys. Lett. **94**, 022102 (2009); 10.1063/1.3059570

Effects of dislocations on electron transport in wurtzite InN
J. Appl. Phys. **103**, 043707 (2008); 10.1063/1.2840051

Electron mobility in InN and III-N alloys
J. Appl. Phys. **102**, 073705 (2007); 10.1063/1.2785005

Low-field electron mobility in wurtzite InN

V. M. Polyakov[a)] and F. Schwierz
FG Festkörperelektronik, Technische Universität Ilmenau, PF 100565, 98684 Ilmenau, Germany

We report on the low-field electron mobility in bulk wurtzite InN at room temperature and over a wide range of carrier concentration calculated by the ensemble Monte Carlo (MC) method. All relevant phonon scatterings are included in the MC simulation. The scattering with ionized impurities is considered in the basic Brooks-Herring and Conwell-Weisskopf formulations. For the steady-state transport, the drift velocity attains a peak value of $\sim 5 \times 10^7$ cm/s at an electric field strength of 32 kV/cm. The highest calculated low-field mobility for undoped InN amounts to $\sim 14\,000$ cm^2/V s at room temperature. We compare our theoretically calculated low-field mobilities with experimental data available in the literature and obtain a quite satisfactory agreement. Finally, an empirical low-field mobility model based on the MC simulation results and experimental mobility data is presented. © *2006 American Institute of Physics.*
[DOI: 10.1063/1.2166195]

During the past few years, InN has attracted considerable attention. Recent progress in InN epitaxial growth has led to monocrystalline wurtzite InN with improved quality, low free electron concentrations, and high mobilities. In particular, the free electron concentration in InN layers grown by molecular beam epitaxy has been reduced to the order of 10^{17} cm^{-3} and electron low-field mobilities above 2000 cm^2/V s have been measured.[1–3] Meanwhile, the best reported mobilities[2] of 3500 cm^2/V s (at room temperature) for samples with electron concentrations between 6×10^{16} and 10^{17} cm^{-3} have reached recent theoretical estimates for the maximum mobility in InN.[4,5]

These experimental results together with the theoretical predictions of the high electron peak drift velocity[6–9] make InN a promising material for high-speed electron devices. There are already first efforts to develop InN high electron mobility transistors.[10,11] To estimate the potential of InN-based high-speed devices, the maximum mobility that can be expected for high quality, low-doped or undoped InN layers is of great importance.

For a long time, a band gap of around 2 eV has been assumed for wurtzite InN. However, recent experimental and theoretical investigations have provided convincing evidence that the band gap of InN is actually about 0.7 eV.[12–15] Consequently, previous Monte Carlo simulations of electron transport in InN (Refs. 6–8) appear to be questionable as they were based on the conduction band structure contradicting to the recent experimental data.[12,13] So far, only one Monte Carlo study using a band structure with the correct band gap[9] has been published. In this work we apply the ensemble Monte Carlo method to investigate the electron transport in bulk wurtzite InN based on the refined band structure. The main emphasis is given to the low-field mobility calculation. The calculated results are compared to recent measured mobility data available in the literature. Also, an empirical model of the room temperature low-field mobility for bulk InN as a function of the carrier concentration is presented.

In the present work, a multivalley approximation to the band structure accounting for the three lowest conduction band minima (Γ_1, Γ_3, and *M-L*) has been employed. Parameters such as effective masses m^*, nonparabolicity factors α for the valleys and valley separation energies have been extracted from the conduction band structure recently calculated by the empirical pseudopotential method.[15] As follows from the analysis of the band structure,[15] electrons can gain a maximum group velocity in the central valley as high as 1.24×10^8 cm/s. This value is a saturation level that is already attained for electron energies of about 1.0 eV. In our band model the satellite valleys Γ_3 and *M-L* are assumed to be parabolic (i.e., $\alpha = 0.0$), while the main Γ_1 valley is taken to be nonparabolic. The Γ_1 valley can be well fitted by

$$\frac{\hbar^2 k^2}{2m^*} = \varepsilon(1 + \alpha\varepsilon) \tag{1}$$

to evaluate the conduction band edge effective mass $m^*_{\Gamma_1} = 0.04 \times m_0$ (m_0 is the rest electron mass) and the nonparabolicity factor $\alpha_{\Gamma_1} = 1.43$ eV^{-1} of the valley. It will be shown later that the satellite valleys do not affect the low-field mobility calculation since no intervalley transfer occurs at low electric fields E. Consequently, the low-field mobility is attributed solely to transport of Γ_1 valley electrons. Table I presents the parameters of the three-valley model of the wurtzite InN band structure applied in this work.

The low-field mobility has been calculated by the simple relation $\mu_0 = v_{\text{drift}}/E$ taken in the linear region of the simulated $v_{\text{drift}}(E)$ curves. As the electric fields used for the calculation of μ_0 are quite low, a long simulation time $T_{\text{sim}} = 15$ ps and a large number of simulated electrons

TABLE I. Spherically symmetric nonparabolic three-valley model of the conduction band structure of wurtzite InN used in the MC simulation.

Conduction band valley	Γ_1	Γ_3	*M-L*
Number of equivalent valleys	1	1	6
Intervalley energy separation (eV)	0.0	1.775	2.709
Effective mass (m^*/m_0)	0.04	0.25	1.00
Nonparabolicity factor (eV^{-1})	1.43	0.0	0.0

[a)]Author to whom correspondence should be addressed; electronic mail: polyakov@e-technik.tu-ilmenau.de

TABLE II. Material parameters of wurtzite InN used in the MC simulation.

Parameter	Value
Mass density (g/cm^3)	6.81
Sound velocity (10^5 cm/s)	3.78
Low-frequency dielectric constant	15.3
High-frequency dielectric constant	8.4
Acoustic deformation potential (eV)	7.1
Polar optical phonon energy (eV)	0.073
Intervalley deformation potential (10^9 eV/cm)	1.0
Intervalley optical phonon energy (eV)	0.073

$N_{sim} = 20\,000$ have been taken to enhance the statistics of the Monte Carlo (MC) calculation of steady-state drift velocity. The interaction of electrons with ionized impurities is taken into account by using the basic Brooks-Herring[16] and Conwell-Weisskopf[17] approaches. Both models are based on the Born and two-body Coulomb interaction approximations, having therefore severe drawbacks to correctly describe electron-ionized impurity scattering over a wide range of impurity concentrations. There is a vast number of attempts to more rigorously investigate electron-impurity interactions (see, e.g., the review by Chattopadhyay and Queisser,[18]) but this issue is beyond the scope of the present study. We also consider InN to be uncompensated and all donors to be ionized at room temperature, thus providing that the ionized impurity concentration is equal to the doping level. Other relevant scattering mechanisms, such as intravalley acoustic phonon, polar optical phonon, and intervalley optical phonon scatterings have been included in the simulation. Table II summarizes the material parameters of wurtzite InN used in the MC simulation.

Figure 1 illustrates the steady-state electron drift velocity in InN calculated as a function of the applied electric field. For comparison, the results for wurtzite GaN are also shown. Remarkable is the higher peak velocity of 5.3×10^7 cm/s reached in InN. In addition, we indicate that the onset of the pronounced negative differential mobility (NDM) region occurs at the substantially lower electric field $E=32$ kV/cm compared to GaN. As clearly observed in Fig. 2, the onset of the NDM is not pinned to the electron intervalley transfer.

FIG. 2. Occupancy of the central (Γ_1) and satellite (Γ_3, M-L) valleys as a function of electric field strength E. The intervalley transfer to the satellite valleys starts at $E=50$ kV/cm, whereas the peak velocity (onset of the NDM) is attained at $E=32$ kV/cm.

Such behavior is different compared to semiconductors, like GaAs, where the NDM is mainly caused by intervalley transfer. In InN the peak velocity is attained at an electric field where all electrons still reside in the central Γ_1 valley. Even at $E=50$ kV/cm, when the drift velocity has already dropped to about 85% of the peak value, only less than 2% of electrons are transferred to the first upper valley. Accordingly, the NDM effect in InN can be attributed to the strong nonparabolicity of the Γ_1 valley, at least, for electric fields when the satellite valleys are not much populated. It should be noted that at higher electric fields the intervalley transfer as an additional mechanism starts increasingly to contribute to the NDM effect. A similar behavior has been reported for electron transport in GaN.[19] Since the low-field mobility is entirely governed by transport of Γ_1 valley electrons, the MC simulation of μ_0 is not sensitive to the parameters of the satellite valleys. In Fig. 3 the calculated low-field mobility μ_0 is shown as a function of ionized impurity concentration n together with the experimental data collected from the literature. It should be noted that the calculated values are drift mobilities whereas the experimental ones are Hall mobilities. We observe that the mobilities calculated using the Brooks-
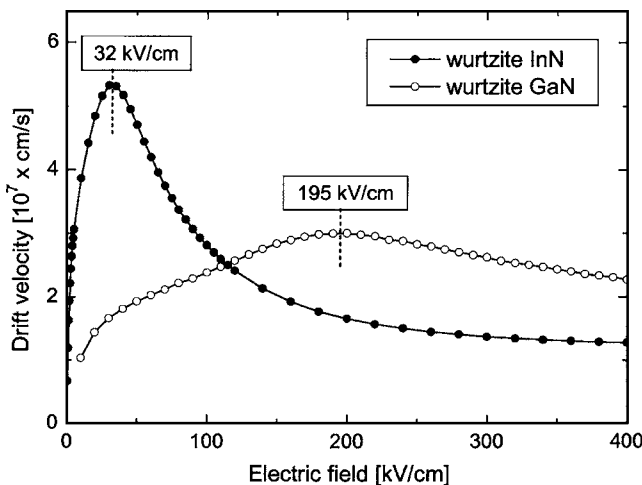

FIG. 1. Calculated steady-state drift velocity as a function of electric field strength for wurtzite InN and GaN (at room temperature). Peak velocities of 5.3×10^7 and 3.0×10^7 cm/s are estimated for InN and GaN, respectively. Ionized impurity concentration is equal to 10^{17} cm^{-3}.
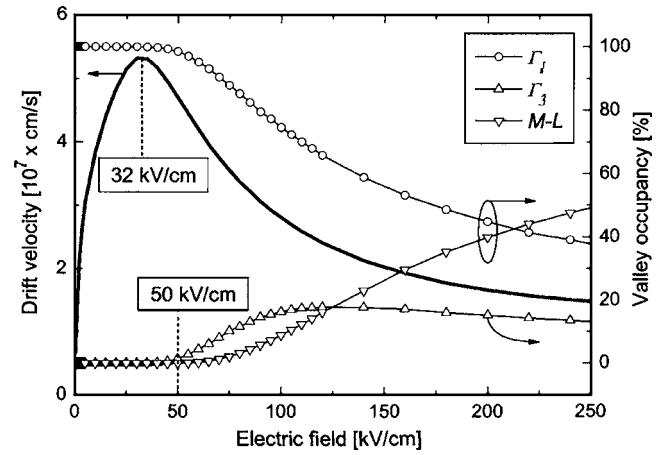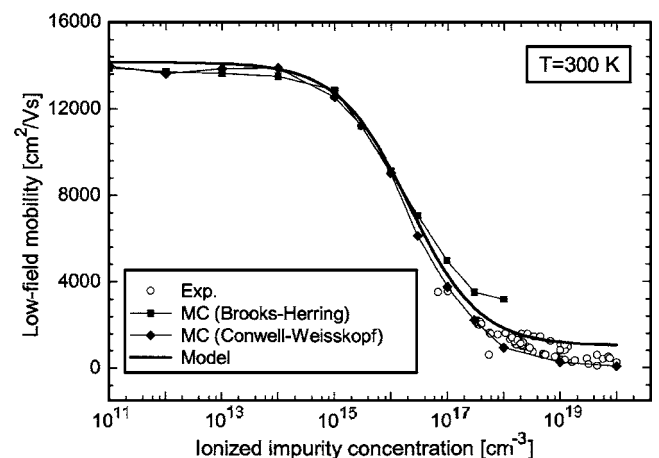

FIG. 3. Calculated low-field electron mobility in wurtzite InN at room temperature: the Brooks-Herring (rectangles) and Conwell-Weisskopf (diamonds) models of ionized impurity scattering. The experimental data (circles) and the empirical model (thick solid line) given by Eq. (2) are also plotted.

Herring and Conwell-Weisskopf models are very close for low impurity concentrations but considerably differ above 5×10^{16} cm^{-3}. Notably, the experimental mobility data are well "captured" by the two simulated curves.

In semiconductor device simulation, empirical mobility models are widely used. A very popular model describing the dependence of the low-field mobility on the carrier density (i.e., on the impurity concentration) is based on an expression proposed by Caughey and Thomas[20]

$$\mu_0 = \mu_{min} + \frac{\mu_{max} - \mu_{min}}{1 + (n/n_{ref})^\beta}, \qquad (2)$$

where μ_{min}, μ_{max}, n_{ref}, and β are fitting parameters. The parameter μ_{max} represents the mobility of undoped samples where lattice scattering is the main scattering mechanism, while μ_{min} is the mobility in highly doped material where impurity scattering is dominant. The parameter β is a measure of how quickly the mobility changes from μ_{min} to μ_{max} and n_{ref} is the carrier concentration at which the mobility is half way between μ_{min} and μ_{max}. Because of the scattering of experimental mobility data and also due to the lack of the data for low carrier concentrations we did not actually try to get a best numerical fit by the least-squares method. We rather attempted to find a reasonable compromise between fitting results, the MC mobility predictions and the tendencies observed for the experimental data. Figure 3 presents the mobility (thick solid line) modeled by Eq. (2) using the following values of the fitting parameters: $\mu_{min} = 1030$ cm^2/V s, $\mu_{max} = 14\,150$ cm^2/V s, $n_{ref} = 2.07 \times 10^{16}$ cm^{-3}, $\beta = 0.6959$.

As shown in Fig. 3, the predicted maximum room-temperature low-field electron mobility in InN is about 14 000 cm^2/V s. This value is considerably above the estimated upper limits of 4000 and 4400 cm^2/V s reported in Refs. 5 and 4, respectively. On the other hand, we consider the high mobilities calculated in the present work to be reasonable because of the following. The effective mass m^* of In$_{0.53}$Ga$_{0.47}$As is $0.041 \times m_0$ (Ref. 21) and high low-field electron mobilities between 10 000 and 15 000 cm^2/V s have been measured in this material (see, e.g., Ref. 22). Bearing in mind that m^* is inversely proportional to μ_0 and that an effective electron mass for InN between $0.04 \times m_0$ and $0.05 \times m_0$ (note the value of $0.04 \times m_0$ used by us) has been recently established,[23–25] the mobilities predicted in this work seem to be realistic.

In summary, electron transport in wurtzite bulk InN at room temperature has been simulated by the ensemble Monte Carlo method. The NDM onset at 32 kV/cm is rather associated with a nonparabolicity of the central Γ_1 valley than with the intervalley transfer. For low doped, uncompensated, dislocation-free material a maximum low-field electron mobility of 14 000 cm^2/V s has been predicted. The high low-field mobility together with the calculated peak velocity of $\sim 5 \times 10^7$ cm/s make InN a very promising material for high-speed electron devices.

[1]W. Walukiewicz, S. X. Li, J. Wu, K. M. Yu, J. W. Ager III, E. E. Haller, H. Lu, and W. J. Schaff, J. Cryst. Growth **269**, 119 (2004).
[2]C. H. Swartz, R. P. Tomkins, T. H. Myers, H. Lu, and W. J. Schaff, Phys. Status Solidi C **2**, 2250 (2005).
[3]F. Chen, A. N. Cartwright, H. Lu, and W. J. Schaff, J. Cryst. Growth **269**, 10 (2004).
[4]V. W. Chin, T. L. Tansley, and T. Osotchan, J. Appl. Phys. **75**, 7365 (1994).
[5]B. R. Nag, J. Cryst. Growth **269**, 35 (2004).
[6]S. K. O'Leary, B. E. Foutz, M. S. Shur, U. V. Bhapkar, and L. F. Eastman, J. Appl. Phys. **83**, 826 (1998).
[7]E. Bellotti, B. K. Doshi, K. F. Brennan, J. D. Albrecht, and P. P. Ruden, J. Appl. Phys. **85**, 916 (1999).
[8]B. E. Foutz, S. K. O'Leary, M. S. Shur, and L. F. Eastman, J. Appl. Phys. **85**, 7727 (1999).
[9]C. Bulutay and B. K. Ridley, Superlattices Microstruct. **36**, 465 (2004).
[10]W. J. Schaff, H. Lu, J. Hwang, and H. Wu, Proceedings of the 7th IEEE/Cornell Conf. "Advanced Concepts in High Performance Devices," 7–9 Aug. 2000, p. 225.
[11]Y.-C. Kong, Y. D. Zheng, C. H. Zhou, Y. Z. Deng, B. Shen, S. L. Gu, R. Zhang, P. Han, R. L. Jiang, and Y. Shi, Solid-State Electron. **49**, 199 (2005).
[12]V. Y. Davydov, A. A. Klochikhin, R. P. Seisyan, V. V. Emtsev, S. V. Ivanov, F. Bechstedt, J. Furthmüller, H. Harima, A. V. Mudryi, J. Aderhold, O. Semchinova, and J. Graul, Phys. Status Solidi B **229**, R1 (2002).
[13]A. A. Klochikhin, V. Y. Davydov, V. V. Emtsev, A. V. Sakharov, V. A. Kapitonov, B. A. Andreev, H. Lu, and W. J. Schaff, Phys. Rev. B **71**, 195207 (2005).
[14]I. Mahboob, T. D. Veal, L. F. J. Piper, C. F. McConville, H. Lu, W. J. Schaff, J. Furthmüller, and F. Bechstedt, Phys. Rev. B **69**, 201307 (2004).
[15]D. Fritsch, H. Schmidt, and M. Grundmann, Phys. Rev. B **69**, 165204 (2004).
[16]H. Brooks and C. Herring, Phys. Rev. **83**, 879 (1951).
[17]E. Conwell and V. P. Weisskopf, Phys. Rev. **77**, 388 (1950).
[18]D. Chattopadhyay and H. J. Queisser, Rev. Mod. Phys. **53**, 745 (1981).
[19]M. Wraback, H. Shen, S. Rudin, E. Bellotti, M. Goano, J. C. Carrano, C. J. Collins, J. C. Campbell, and R. D. Dupuis, Appl. Phys. Lett. **82**, 3674 (2003).
[20]D. M. Caughey and R. E. Thomas, Proc. IEEE **52**, 2192 (1967).
[21]Y. A. Goldberg and N. M. Shmidt, in *Handbook Series on Semiconductor Parameters*, edited by M. Levinshtein, S. Rumyantsev, and M. Shur (World Scientific, Singapore, 1999), Vol. 2.
[22]Ch. Köpf, H. Kosina, and S. Selberherr, Solid-State Electron. **41**, 1139 (1997).
[23]B. R. Nag, Phys. Status Solidi B **237**, R1 (2003).
[24]S. P. Fu and Y. F. Chen, Appl. Phys. Lett. **85**, 1523 (2004).
[25]B. Arnaudov, T. Paskova, P. P. Paskov, B. Magnusson, E. Valcheva, B. Monemar, H. Lu, W. J. Schaff, H. Amano, and I. Akasaki, Phys. Rev. B **69**, 115216 (2004).